Temperature dependence of elastic constants in unidirectional carbon fiber reinforced shape memory polymer composites

Fengfeng Li [a, b], Jinsong Leng [c], Yanju Liu [a, *], Chrystel Remillat [b], Fabrizio Scarpa [b, *]

a. Department of Astronautical Science and Mechanics, Harbin Institute of Technology (HIT), P.O. Box 301, No. 92 West Dazhi Street, Harbin 150001, People's Republic of China

b. Bristol Composites Institute (ACCIS), University of Bristol, Bristol BS8 1TR, UK

c. National Key Laboratory of Science and Technology on Advanced Composites in Special Environments, P.O. Box 3011, No. 2 YiKuang Street, Harbin 150080, People's Republic of China

** corresponding author at: Department of Astronautical Science and Mechanics of Harbin Institute of Technology, Harbin 150001, People's Republic of China* and *Bristol Composites Institute (ACCIS)of University of Bristol, Bristol BS8 1TR, UK. Email addresses: yj_liu@hit.edu.cn (Y. Liu), F.Scarpa@bristol.ac.uk (F. Scarpa)*

Abstract: The work describes a model to predict the elastic constants of unidirectional carbon fiber reinforced shape memory polymer composites (SMPCs) with different fiber volume fractions within the temperature range of 293 K to 393 K. The model is based on a theoretical description of the phase transition of the shape memory polymer (SMP). Two glassy phase volume fraction functions are developed, one based on the Eyring equation, the other based on the normal distribution equation. The longitudinal and transverse moduli, axial and transverse shear moduli, and axial Poisson's ratio are derived by using the glassy phase volume fraction function and modified rule of mixture. The axial Poisson's ratio increases with the temperature increase, while the other four constants decrease nonlinearly with rising temperatures. An inverse identification of the elastic constants at different temperature via numerical and experimental modal analysis from a flat SMPC laminate shows that the model proposed is adequate to describe the temperature

dependence of the elastic constants of the laminate.

Keywords: shape memory polymer composite, carbon fiber, temperature dependence, elastic constants

1. Introduction

Polymeric composites have been widely used in civil, automotive, and aerospace applications due to their easy processing, high specific strength and stiffness, tunable properties, good corrosion resistance and low cost [Feng and Guo, 2016; Gibson et al., 2006; Guo et al., 2013]. Their properties can be tailored by varying the type, content and distribution of the matrix and reinforcement [Feng and Guo, 2016; Gibson et al., 2006; Guo et al., 2013]. These composites possess temperature-dependent mechanical properties due to the viscoelastic nature of the polymeric matrix [Feng and Guo, 2016; Haque et al., 1991; Odegard and Kumosa, 2000; Yoon and Kim, 2000]. With the increase in temperature the matrix becomes compliant, resulting in a decrease of the magnitude of the stiffness within the glass transition temperature range. This is particularly evident for matrix-dominated constants such as the transverse and shear moduli [Mahieux and Reifsnider, 2001]. It is therefore essential to possess a systematic and reliable database of mechanical properties for composites at different temperatures. In that sense, a significant body of work has been devoted to characterizing the relationship between mechanical properties and temperature of different composites.

Gibson et al. have investigated the use of laminate theory for composites subjected to load in fire conditions [Gibson et al., 2006]. In that work the Authors carried out tensile and compression tests on polyester/woven E-glass laminates and found that the longitudinal, transverse and in-plane shear moduli, the tensile and compressive strengths show a hyperbolic-type dependence versus the temperature. Gou et al. have analyzed the static and dynamic behavior of cross-ply and unidirectional glass/epoxy laminates by using dynamic mechanical analyzer (DMA) techniques [Guo et al., 2013]. The storage and static moduli showed a similar sensitivity to temperatures with a severe drop occurring during the glass transition. Feng et al. further studied the temperature and frequency-dependent mechanical properties of glass/epoxy composites [Feng and Guo, 2016]. The loss factor, storage and loss moduli were measured between 310 K and 390 K at 1, 5, 10, 40, 100, and 160 Hz. The modulus-temperature curves measured in that work are similar to the ones obtained by Gou et al. but shift to the right with the frequency increase. Haque et al. have

evaluated the temperature and moisture-induced degradation of the uniaxial (longitudinal) mechanical properties in Kevlar 49 and T-300 reinforced epoxy-based single or hybrid fiber composites [Haque et al., 1991]. This study showed that the degradation of the tensile modulus of these composites was mainly due to the temperature. The tensile modulus decreased with the temperature increase, on the opposite the Poisson's ratio tended to increase with higher temperatures. Yoon et al. have evaluated the change of the elastic properties in carbon/epoxy composites with 58% of fiber volume fraction and a glass transition temperature (T_g) of 110 ºC [Yoon and Kim, 2000]. In that case, the longitudinal modulus and the Poisson's ratio remained nearly constant when the temperature increased from 25 ºC to 140 ºC, whereas the transverse and shear moduli linearly decreased with the increase of temperature. These elastic parameters were fitted as linear functions of the temperature for formulation convenience. Odegard et al. have studied mechanical properties of a unidirectional carbon/PMR-15 composite (T_g 310 ºC) by using tensile tests [Odegard and Kumosa, 2000]. Significant reductions of longitudinal, transverse, and shear moduli were observed with temperatures between 27 ºC and 316 ºC. Although the Poisson's ratio has been approximated as a constant by linear curve fitting, the results still showed that the average Poisson's ratio at room temperature was lower than the one at 316 ºC.

Shape memory polymer composites (SMPCs) are polymeric composites that possess shape memory due to their matrix. Shape Memory Polymers (SMPs) can be transferred from a temporarily deformed shape to the original shape under external stimuli [Leng et al., 2011; Lu et al., 2018; Yang and Li, 2016]. The fundamental mechanism behind the shape memory behavior is the activation and freeze of the motion of the SMP chains above and below the T_g [Lu et al., 2018; Yang and Li, 2016]. In recent years, smart materials and structures have been developed and applied to aerospace due to their intrinsic advantages in terms of lightweight, high specific strength and stiffness, large recoverable deformation and high recovery rate [Herath et al., 2018; Li et al., 2019b]. The use of SMPCs in space structures such as deployable solar arrays, trusses, antennas, and intelligent release devices is also increasing [Barrett et al., 2006; Dao et al., 2018; Li et al., 2016]. Most of the SMPCs in aerospace applications are continuous fiber reinforced composites, normally carbon fiber or fabric, and this is due to their good chemical and

physico-mechanical properties [Barnes and Cogswell, 1989; Dao et al., 2018; Herath et al., 2018; Li et al., 2016; Li et al., 2019b]. Any spacecraft in orbit must withstand large temperature differences because the spacecraft needs to move in and out of the earth's shadow [Barnes and Cogswell, 1989; Li et al., 2019a]. The temperature variation affects the mechanical behavior of SMPCs due to the temperature-dependent mechanical properties of the matrix [Feng and Guo, 2016; Gibson et al., 2006; Guo et al., 2013; Haque et al., 1991; Mahieux and Reifsnider, 2001; Odegard and Kumosa, 2000; Yoon and Kim, 2000]. In particular, the modulus of SMPCs could vary at least one order of magnitude at low and high temperatures, if the temperature change covers the glass transition range of the matrix [Leng et al., 2011; Li et al., 2019a; Li et al., 2019b]. Therefore, it's important to determine the relationship between elastic constants and temperature in the full range of glass transition.

Although most of the models used to predict the modulus of polymeric composites are not specifically developed for SMPCs, we can still draw inspiration from previous studies since the SMP matrix is a polymer. This study aims at providing a model to predict the elastic constants of the unidirectional fiber reinforced SMPCs and therefore to determine the laminate stiffness at various temperatures for different fiber volume fractions. Section 2 reviews existing studies related to the description of the relationship between elastic constants and temperature in polymeric composites. The model for the unidirectional fiber reinforced SMPC is developed in section 3. Two glass phase volume fraction equations, one based on the Eyring equation and the other based on the normal distribution function, are established for the temperature dependence of the SMP matrix. Five independent elastic constants (longitudinal modulus E_{11}, transverse modulus E_{22}, axial shear modulus G_{12}, axial Poisson's ratio ν_{12}, transverse shear modulus G_{23}) are then derived since the unidirectional fiber reinforced laminate possesses transverse isotropy. Section 4 shows the validation of the model. Validations using experimental and other theoretical data are here limited to the glass phase volume fraction equations and longitudinal modulus. Other elastic constants are parametrically investigated. Comparisons of the elastic constants with different glass phase volume fraction equations are also presented. Section 5 presents the inverse identification of the elastic constants via numerical and experimental modal

analysis of a plain weave carbon fabric reinforced SMPC laminate at elevated temperatures. Conclusions are reported in Section 6.

2. Relationship between the composites elastic constants and the temperature

Several theoretical models with different complexity and variable accuracy have been developed to predict the Young's modulus in composites as a function of temperature. These models usually are developed or benchmarked for the longitudinal modulus (i.e., the 0° angle in a unidirectional laminate). Most existing thermal mechanical models involve temperature-dependent elastic constants developed as empirical functions by fitting experimental results at specific collected points. Gibson et al. established a hyperbolic tanh function to compute the elastic constants in terms of resin content and temperature [Gibson et al., 2006].

$$E(T) = \frac{E_U + E_R}{2} - \frac{E_U - E_R}{2} \tanh(\kappa(T - T')) \tag{1}$$

where E_R and E_U are the relaxed (at high temperature) and unrelaxed (at low temperature) moduli, κ is the constant describing the abruptness of the modulus transition, T' is the glass transition temperature.

Guo et al. devised a relatively simple temperature-dependent model to estimate the dynamic storage and static flexural moduli [Guo et al., 2013]. Only the longitudinal modulus of glass/epoxy laminates are presented there:

$$E(T) = E_g - \frac{E_g - E_r}{e^{-\lambda \cdot (T - T_g)} + 1} \tag{2}$$

In Eq. (2), E_g and E_r are the modulus of the composite in glassy and rubbery phases, T_g is the glass transition temperature, λ is the rate of increase of the amount of molecules per unit temperature in rubbery phase.

Gu et al. also proposed an empirical model of the temperature-dependent Young's modulus in a phenomenological form [Gu and Asaro, 2005]. The model is suitable for simple temperature field. When the temperature field is in a complex form, it is impossible to theoretically evaluate the modulus variation:

$$E(T) = E_0\left(1-\frac{T-T_r}{T_{ref}-T_r}\right)^{\chi} \tag{3}$$

where E_0 is the modulus at ambient temperature, T_r is the room temperature, T_{ref} is the reference temperature at which the modulus vanishes, χ is the power law index.

3. Theory

In our model, the SMP in the composite is characterized by using the phase transition concept, for which the rubbery and glassy phases can transform into each other upon temperature change [Lu et al., 2018; Volk et al., 2010; Yang and Li, 2016]. Fig. 1 shows the schematics of the phase transition schematic in a long fiber reinforced unidirectional aligned and uniformly distributed SMPC. Besides the rubbery and glassy phases, the fiber is considered as a phase in the model. Although the fiber properties are assumed to be temperature independent, the SMPC possesses temperature-dependent properties due to the SMP matrix, and the transition between the rubbery phase and the glassy phase provides the temperature variation of the elastic constants.

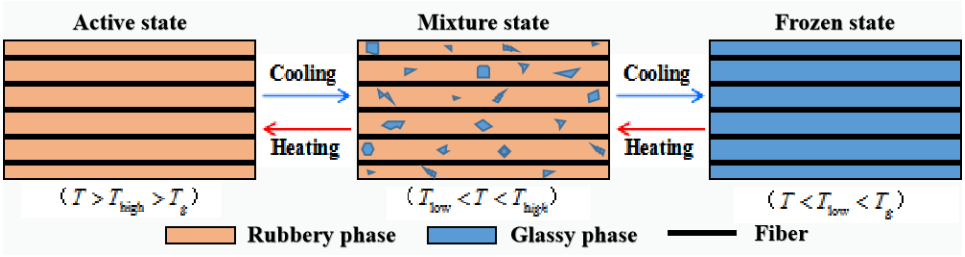

Fig. 1. Schematic of the phase transition model for the unidirectional fiber reinforced SMPC

To model the elastic constants of the unidirectional fiber reinforced SMPC we impose the

following assumptions [Mendels et al., 1999]:

· The fiber is continuous and extends to the length of the composite;

· The fiber is aligned in the longitudinal direction only;

· Fiber properties are independent of temperature;

· The mechanical properties of the matrix are temperature-dependent;

· The temperature is homogeneous at every location of the composite;

· Only linear elastic and small deformations for the matrix and the fiber are allowed (i.e., tensile and compressive modulus coincide).

The longitudinal direction of the fiber reinforced composite is the direction parallel to the fibers (i.e., the 1-direction). The transverse direction is perpendicular to the longitudinal direction. Since there are two mutually perpendicular transverse directions, they are denoted as 2 and 3, respectively.

3.1 Glassy phase volume fraction function

3.1.1 Glassy phase volume fraction function based on Eyring equation

The glassy phase volume fraction $\phi_g(T)$ is often introduced to describe the phase transition upon temperature changes [Leng et al., 2011; Lu et al., 2018; Volk et al., 2010; Yang and Li, 2016]. The function $\phi_g(T)$ is equal to 0 when the SMP is at rubbery phase and to 1 in glassy phase. We use the symbol γ to describe the probability of the phase transition. The $\phi_g(T)$ can be therefore written as:

$$\phi_g(T) = 1 - \gamma(T) \tag{4}$$

The probability $\gamma(T)$ is a modified Eyring equation, as shown in Eq. (5). The modification

is performed because the activation of the polymer chains under an external stress field reduces the total activation energy (i.e., the energy required from the glassy phase to the rubbery phase), which equals to the product of the volume activated by the effective stress and the effective stress [Dotsenko, 1979]:

$$\gamma(T) = kT \exp\left(-\frac{\Delta G(T) - \sigma V}{RT}\right) \tag{5}$$

In Eq. (5), k is the correction constant, T is the absolute temperature, $\Delta G(T)$ is the change of activation energy (Gibbs energy), σ is the effective stress, V is the activation volume, R is the gas constant which equals 8.314 J/(mol·K). The change of the Gibbs activation energy $\Delta G(T)$ is calculated following the Williams-Landel-Ferry (WLF) relation [Lu et al., 2018]:

$$\Delta G(T) = \Delta G(T_g) \cdot 10^{\frac{-C_1(T-T_g)}{C_2+T-T_g}} \tag{6}$$

where $\Delta G(T_g)$ is the activation energy, C_1 and C_2 are the WLF constants for the glass transition temperature T_g.

The stress σ is the difference between the applied stress and the internal stress σ_i. During a free recovery process, the applied stress equals to zero and $\sigma = \sigma_i$. An empirical equation of the effective stress versus the external applied one is [Dotsenko, 1979]:

$$-\dot{\sigma}_i = A(\sigma)^p \tag{7}$$

where A and p are parameters.

The activation volume V can be obtained by plotting the logarithm of the stress relaxation rate versus stress at a specific temperature and a constant m [Dotsenko, 1979]:

$$V = mT\left[\frac{\partial \ln(-\dot{\sigma}_i)}{\partial \sigma_i}\right]_T \tag{8}$$

Substituting the logarithm of Eq. (7) into Eq. (8) we obtain:

$$V = mT\frac{p}{\sigma} \tag{9}$$

Substituting Eqs. (5, 6, 9) to Eq. (4), the new glassy phase volume fraction function is:

$$\phi_g(T) = 1 - kT\exp\left[-\frac{\Delta G(T_g)\cdot 10^{\frac{-C_1(T-T_g)}{C_2+T-T_g}}}{RT} + n\right] \tag{10}$$

where $n = \frac{mp}{R}$. This new glassy phase volume fraction function (10) can be used to represent SMPCs since the temperature dependence is dominated by the SMP matrix. The parameters k, $\Delta G(T_g)$, C_1, C_2 and n used for adjusting the shape of the curve can be got by curve fitting. To simplify the determination of k, $\Delta G(T_g)$ and C_2 we recommend to adopt the values of C_1 and n close to the empirical values of 16 and 1, respectively [Angell, 1997; Lu et al., 2018].

3.1.2 Glassy phase volume fraction function based on a normal distribution function

Most glassy phase volume fraction functions are empirical formulas with different forms [Lu et al., 2018; Volk et al., 2010; Yang and Li, 2016]. Unlike equations with physical meaning, such as the glass transition function based on the Eyring equation above, empirical functions are simpler but more specific to certain situations. An example is Eq. (11), which is based on a normal distribution function:

$$\phi_g(T) = 1 - \frac{1}{\omega\sqrt{\frac{\pi}{2}}}\int_{T_{\min}}^{T}\exp\left[\frac{-2(t-T_g)^2}{\omega^2}\right]dt \tag{11}$$

In Eq. (11), ω is a scaling factor for adjusting the shape of the hyperbolic curve, which is

obtained from curve fitting. The lower limit of the integration $T_{\min}$ is the minimum temperature during the experiments. It could also be set to negative infinity, the same as in the normal distribution function. For reducing the computational cost, the lower limit is here set to be $T_{\min}$. As it will be shown in section 4.1, the value of ω assumes slightly different values hether using the negative infinity or a finite temperature.

3.2 Longitudinal modulus

The glass transition of the composite can be correlated to the variation of its modulus versus the temperature. The glassy phase volume fraction is derived in Eq. (12) from [Bai et al., 2008; Guo et al., 2013]:

$$\phi_g(T) = \frac{E(T) - E_{T_H}}{E_{T_L} - E_{T_H}} \tag{12}$$

In Eq. (12), $\phi_g(T)$ is the glassy phase volume fraction of the temperature-dependent modulus $E(T)$; E_{T_H} and E_{T_L} are the moduli at high temperature T_H ($T_H > T_g$) and low temperature T_L ($T_L < T_g$), respectively. When the composite is at T_L the matrix of the SMPC is in glassy phase $\phi_g(T_L) = 1$. When the matrix is in rubbery phase, the glass transition function becomes $\phi_g(T_H) = 0$. By placing $E(T)$ to the left side of Eq. (12), the instantaneous modulus in a function of temperature is given by the following expression:

$$E(T) = (E_{T_L} - E_{T_H})\phi_g(T) + E_{T_H} \tag{13}$$

3.2.1 Longitudinal modulus at low temperature (below T_g)

The modulus of a SMP tends to differ by two orders of magnitude at temperatures below and above the T_g [Li et al., 2019a]. At a low temperature T_L (the room temperature in our case),

the modulus of the SMP has a magnitude of 10^0 GPa [Li et al., 2019a]. Although the modulus of the matrix is also two orders of magnitude lower than the the one of carbon fibers, the rule of mixture (ROM) to estimate the modulus of the overall composite can still be used [Subramanian, 1994]. To calculate the modulus along the longitudinal direction, the classical ROM assumes that the matrix and fiber have the same strain, but the displacement of the fiber cannot be equal to the one of the matrix unless a perfect bond is present. We use here a refined ROM model as proposed by Subramanian by introducing a efficiency factor α to describe the load transfer from the matrix to the fiber [Subramanian, 1994]:

$$\varepsilon_{11}^{f} = \alpha \varepsilon_{11}^{m} \tag{14}$$

The longitudinal modulus of the SMPC at low temperature is then obtained as:

$$E_{11\_T_L} = \frac{V_m E_{m\_T_L} + \alpha V_f E_f}{V_m + \alpha V_f} \tag{15}$$

In (15) $E_{11\_T_L}$ and $E_{m\_T_L}$ are the longitudinal modulus of the composite and the matrix at temperature T_L and E_f is the fiber modulus. When $\alpha = 0$ (i.e., no transfer between matrix and fiber) we have $E_{11\_T_L} = E_m$; when $\alpha = 1$ (i.e., perfect bonding) $E_{11\_T_L} = V_m E_{m\_T_L} + V_f E_f$.

3.2.2 Longitudinal modulus at high temperature (above T_g)

At high temperature (above T_g) the matrix is in a rubbery phase, and its modulus varies between 10^0-10^1 MPa, which is significantly lower than that of the carbon fiber [Li et al., 2019a]. The load at T_H is mainly supported by the carbon fiber in tension. When $V_f \to 1$, the modulus of composite $E_{11\_T_H}$ is approximately equal to fiber one ($E_{11\_T_H} \approx E_f$). When $V_f \to 0$, the modulus is $E_{11\_T_H} \approx E_{m\_T_H}$. The modulus of the composite at T_H can be therefore assumed as:

$$E_{11\_T_H} = E_{m\_T_H} + \beta E_f V_f^{\eta} \tag{16}$$

where β, η are the fiber-dominated efficiency factors, serving as curve-fitting coefficients for experimental results.

3.2.3 Longitudinal modulus E_{11}

Substituting (15), (16) into Eq. (13), the volume fraction and temperature-dependent longitudinal modulus of the unidirectional fiber reinforced SMPC can be written as:

$$E_{11}(T)=\left[\frac{V_m E_{m\_T_L}+\alpha V_f E_f}{V_m+\alpha V_f}-(E_{m\_T_H}+\beta E_f V_f^{\eta})\right]\phi_g(T)+(E_{m\_T_H}+\beta E_f V_f^{\eta}) \tag{17}$$

This equation involves the identification of three fitting parameters (α, β, η), for which tests on several fiber volume fraction composites at both low and high temperatures are needed. If the fiber volume fraction is not considered, one can use Eqs. (10, 11, 13) to evaluate the temperature dependence of the modulus for a certain type of composite. In that case, only the modulus of the matrix is needed as a function of temperature (examples are presented in the Appendix. A).

3.3 Other independent elastic constants (E_{22}, G_{12}, ν_{12}, G_{23})

The transverse modulus E_{22} and the shear modulus G_{12} are derived by replacing the constant modulus with the temperature-dependent modulus of the matrix in Halpin-Tsai equations [Pegoretti et al., 2002]:

$$E_{22}=E_m(T)\frac{1+2\xi V_f}{1-\xi V_f} \tag{18a}$$

$$\xi=\frac{E_f-E_m(T)}{E_f+2E_m(T)} \tag{18b}$$

$$E_m(T)=(E_{m\_T_L}-E_{m\_T_H})\phi_g(T)+E_{m\_T_H} \tag{18c}$$

where ξ is the effective factor, $E_m(T)$ is the modulus of the matrix calculated by Eq. (13).

$$G_{12} = G_m(T)\frac{1+\zeta V_f}{1-\zeta V_f} \tag{19a}$$

$$\zeta = \frac{G_f - G_m(T)}{G_f + G_m(T)} \tag{19b}$$

$$G_m(T) = \frac{E_m(T)}{2(1+\nu_m(T))} \tag{19c}$$

where $G_m(T)$ is the shear modulus of the matrix, ζ is the effective factor, G_f is the shear modulus of the fiber and $\nu_m(T)$ is the matrix's Poisson's ratio. We consider here the Poisson's ratio of the epoxy-based SMP with values ranging between 0.35 and 0.5 at low and high temperatures [McClung et al., 2012]. An interpolation between the two extremes is defined as a sigmoidal form [McClung et al., 2012; Mott et al., 2008; Pandini and Pegoretti, 2008]:

$$\nu_m(T) = (1-\phi_g(T))(\nu_m(T_H) - \nu_m(T_L)) + \nu_m(T_L) \tag{20}$$

where $\nu_m(T_H)$ and $\nu_m(T_L)$ are the Poisson's ratios of the matrix at high and low temperatures, respectively.

The axial Poisson's ratio of the SMPC $\nu_{12}(T)$, is calculated using the ROM approach:

$$\nu_{12}(T) = \nu_m(T)V_m + \nu_f V_f \tag{21}$$

where ν_f is the Poisson's ratio of fiber.

The transverse shear modulus G_{23} is obtained by replacing the elastic constants E_{11}, E_{22}, and ν_{12} with temperature-dependent terms in the equation proposed by Christensen [Christensen, 1988]:

$$G_{23}(T) = \frac{(1-\nu_{12}(T))E_{22}(T)}{2\left(1-\frac{\nu_{12}^2(T)E_{22}(T)}{E_{11}(T)}\right)} \tag{22}$$

4. Validation

Here we use the results from isothermal three-point bending tests carried out on unidirectional carbon fiber reinforced epoxy-based SMPCs with fiber mass fractions of 23%, 30%, 37% in reference [Li et al., 2019b]. We calculate the relation between mass fraction and volume fraction as:

$$\phi_f = \frac{\rho_m \varphi_f}{\rho_m \varphi_f + \rho_f (1-\varphi_f)} \tag{23}$$

where ϕ_f, φ_f are the fiber volume fraction and fiber mass fraction, respectively; ρ_m is the density of the epoxy-based SMP matrix (1.2 g/cm^3) and ρ_f is the density of carbon fiber (1.8 g/cm^3). By calculation, the fiber mass fractions of 23%, 30%, and 37% correspond to fiber volume fractions of 17%, 22%, and 28%.

Table 1. Mechanical properties of the carbon fiber and epoxy-based SMP [Li et al., 2019b; Miyagawa et al., 2005]

Materials	E_{11} (MPa)	E_{22} (MPa)	G_{12} (MPa)	ν_{12}	G_{13} (MPa)	G_{23} (MPa)
Carbon fiber (T300)	230000	8000	27300	0.256	27300	3080
Epoxy resin (293 K)	1950	\	720	0.35	\	\
Epoxy resin (393 K)	8.17	\	2.81	0.5	1	1

The mechanical properties of the T300 carbon fiber and the epoxy based SMP matrix are listed in Table 1. And the carbon fiber maintains constant mechanical properties over the temperature range of 293 K to 393 K [Miyagawa et al., 2005; Sauder et al., 2004].

4.1 Glassy phase volume fraction transformation

The temperature-dependent characteristics of the SMPC are intrinsic to the behavior of its modulus. Here we use the flexural modulus in reference [Li et al., 2019b] to empirically obtain the glassy phase volume fraction transformation with the change of temperature. By substituting the modulus in Eq. (12), the normalized flexural modulus is obtained, and it can be used to determine the parameters in Eqs. (10, 11). The normalized experimental data of the SMPCs with different fiber volume fractions are substantially identical (Fig. 2), indicating that the matrix dominates the temperature-dependent characteristics. Eqs. (10, 11) obtained from user defined functions from the Origin software are used to fit the scatters.

In Eq. (10), the values of $\Delta G(T_g)$, C_1, C_2 are 1312 J/mol, 16, and 571 K at the glass transition temperature $T_g = 333\mathrm{K}$, respectively. The parameters k, R and n are equal to 0.001 K^{-1}, 8.314 J/(mol·K) and 1, respectively. Fig. 2 (a) shows the fitting curve with the coefficient of determination (R^2) of 97.6%. The residuals with a confidence level of 95% are also presented in Fig. 2 (a).

With ω, $T_{\min}$ are equal to 33.1 and 293 in Eq. (11); the fitting curve is plotted in Fig. 2 (b) with the R^2 of 99.0%. When $T_{\min}$ tends to $-\infty$, the value of ω changes to 33.05 for obtaining the same previous R^2 and curve shape. The difference in values of ω in these two lower integration limit cases is ~0.15%. The finite value $T_{\min} = 293\mathrm{K}$ is finally chosen to reduce the computational cost.

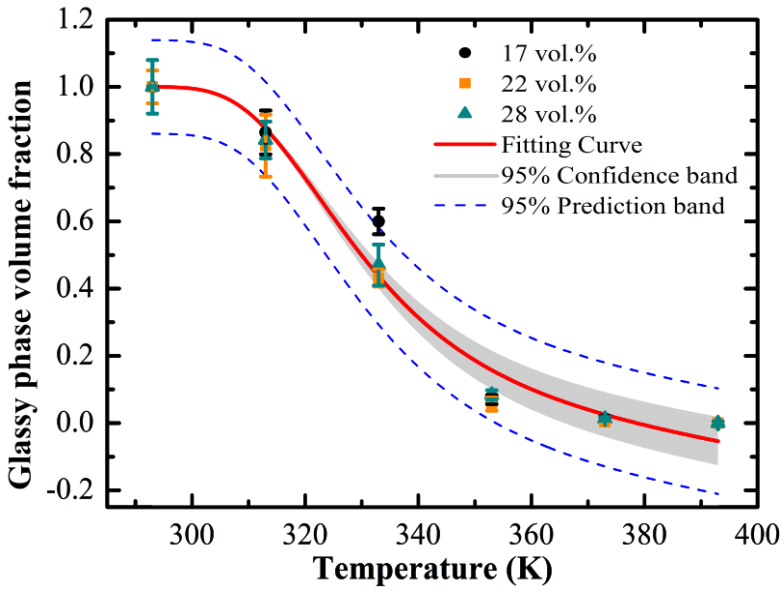

(a)

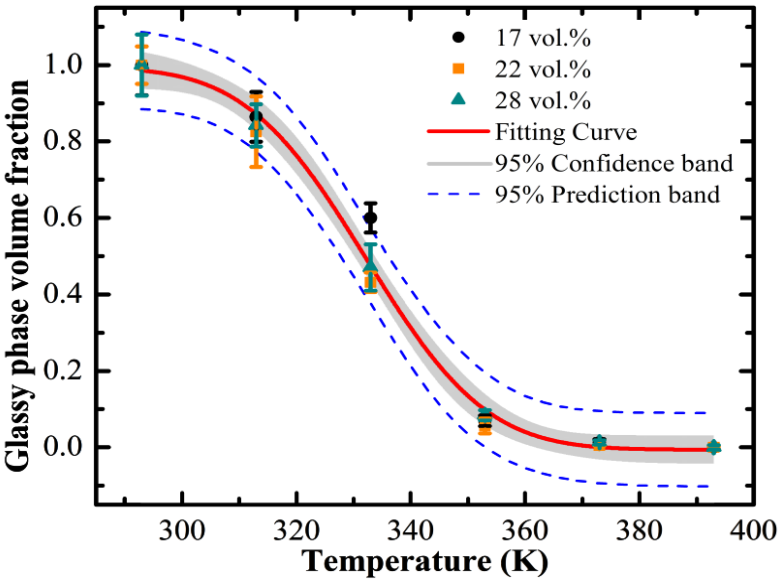

(b)

Fig. 2. Glassy phase volume fraction transformation,

(a) $\phi_g(T)$ by Eq. (10), (b) $\phi_g(T)$ by Eq. (11)

Fig. 2 (a) shows some discrepancies between the numerical data from the experimental results at temperatures above T_g. The poor fitting at high temperature can affect the subsequent

prediction of the elastic constants. The predicted glassy phase volume fraction transformation curve in Fig. 2 (b) fits well with the experimental results in the whole temperature range. The curve obtained by Eq. (11) inherits the characteristics of the normal distribution function, with the slopes at temperatures being symmetrical to the T_g value. The Eyring-based Eq. (10) is however more suitable for curves with unsymmetrical slopes around the T_g.

4.2 Longitudinal modulus

The flexural modulus in Fig. 5 (a) of reference [Li et al., 2019b] is used to verify the accuracy of the model related to the longitudinal (axial) modulus. The modulus has an almost linear dependency versus the fiber volume fraction around 293 K. The parameter α obtained by inserting the values of $E_{m\_T_L}$ and E_f from Table 1 into Eq. (15) is equal to 0.63. The longitudinal modulus of the SMPCs at 393 K are one order of magnitude lower than the one at 293 K. By fitting the data using Eq. (16), the parameters β and η are identified as $\beta = 0.52$ and $\eta = 1.3$. The temperature-dependent modulus for various fiber volume fractions shown in Fig. 3 is obtained by inserting the values of α, β and η, and substituting the glassy phase volume fraction Eqs. (10, 11) into Eq. (17).

Fig. 3 (a) shows the curve based on the glassy phase volume fraction Eq. (10) agrees well with the experimental data related to the 22 vol.% and 28 vol.% SMPCs at 293 K, 313 K, 333 K and 373K. The error however exceeds 45% at 353 K and 393 K. The curve for the 17 vol.% SMPC case follows the same trend as the experimental data; the errors at 293 K, 313 K and 373 K are lower than 5% and over 21% at other temperatures. The longitudinal modulus is obviously directly proportional to the fiber fraction. The modulus of the 22 vol.% SMPC at 293 K is 34 % higher than the one of 17 vol.%. The modulus of the 28 vol.% SMPC is however 69% higher than the one with 17 vol.% at 293 K.

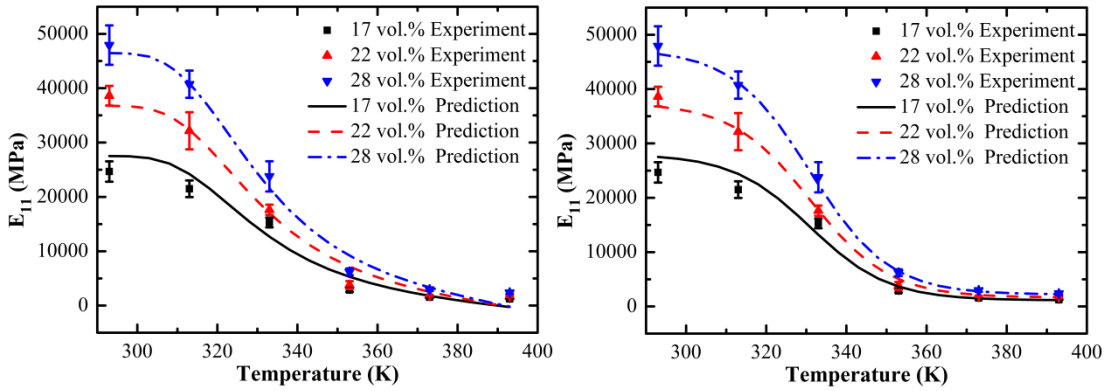

(a) (b)

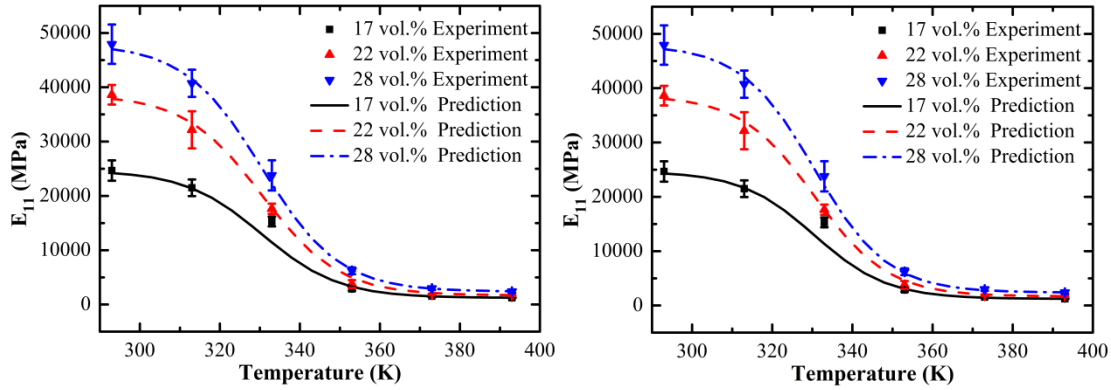

(c) (d)

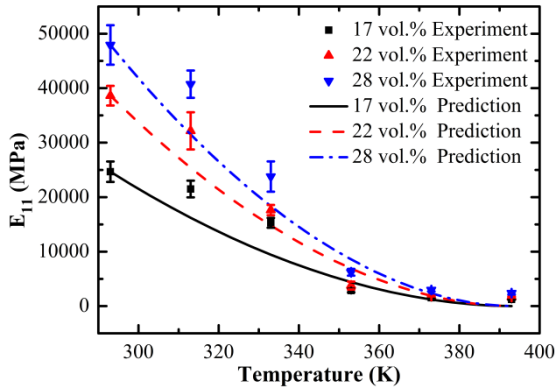

(e)

Fig. 3. The flexural moduli E_{11} of SMPCs with different fiber volume fractions at different temperatures, (a) prediction based on Eq. (10), (b) prediction based on Eq. (11), (c) prediction based on Eq. (1), (d) prediction based on Eq. (2), (e) prediction based on Eq. (3)

Fig. 3 (b) shows the curve with the glassy phase volume fraction obtained by Eq. (11) features a hyperbolic tangent decrease with the temperature. The numerical results fit well to the experimental data for the 22 vol.% and 28 vol.% SMPCs, with error being less than 10% at all specified temperatures. The numerical results for the 17 vol.% SMPC at 293 K, and 313 K are significantly higher than the experimental ones, but lower at 333 K. The discrepancy is never higher than 15%. At 293 K, the moduli for the 22 vol.% and 28 vol.% SMPCs are 34% and 69% higher than the analogous value for 17vol.%; at 393 K, the increases are 45% and 94%, respectively.

The predicted longitudinal modulus based on the normal distribution equation shows better compliance to the experimental results than the one based on the Eyring equation. The difference between the two predictions is similar to the difference of the glassy phase volume fraction transformation curves (Fig. 2) obtained by Eqs. (10, 11). We have also compared the longitudinal modulus predicted by Eqs. (1-3) with material parameters listed in Table 2. It's worth noticing that the model proposed in this study is determined solely by matrix and fiber parameters; Eqs. (1-3) however necessitate the knowledge of the moduli of the composite at 293 K or 393 K. Although the curves calculated by Eqs. (1-2) provide a good fit (Figs. 3 (c) and (d)), the model used in this study could also provide a similar accuracy by using the modulus at extreme temperatures in Eq. (13). Curves obtained by using Eq. (3) do not show a hyperbolic trend (Fig. 3 (e)).

Table 2. The material parameters in Eqs. (1-3, 16)

Material parameters		Values	Units	Description
E_U, E_g, E_0	17 vol.%	24669	[MPa]	Longitudinal modulus at 293 K in Eqs. (1-3).
	22 vol.%	38618	[MPa]	
	28 vol.%	47927	[MPa]	
E_R, E_r	17 vol.%	1218	[MPa]	Longitudinal modulus at 393 K in Eqs. (1, 2).
	22 vol.%	1679	[MPa]	
	28 vol.%	2377	[MPa]	
$E_{m\_T_H}$		8.17	[MPa]	Epoxy resin modulus at 393 K.
$E_{m\_T_L}$		1950	[MPa]	Epoxy resin modulus at 293 K.

E_f	230000	[MPa]	Modulus of the carbon fiber.
$T^{'}$	330.5	[K]	Glass transition temperature in Eqs. (1, 2).
T_r	293	[K]	Room temperature in Eq. (3).
T_{ref}	393	[K]	Reference temperature in Eq. (3).
α	0.63	[-]	Transfer factor in this work.
β	0.52	[-]	Efficiency factor in this work.
η	1.3	[-]	Efficiency factor in this work.
κ	0.052	[-]	Sharpness constant in Eq. (1).
λ	0.11	[-]	Growth rate in Eq. (2).
χ	1.88	[-]	Power law index in Eq. (3).

4.3 Other elastic constants

The transverse modulus E_{22} and the axial shear modulus G_{12} are calculated by using Eqs. (18, 19) and related parameters in Table 1. The E_{22} and G_{12} with the two glassy phase volume fraction functions (10) and (11) are substantially the same at temperatures below T_g. These two elastic constants based on the Eyring equation however exhibit negative values above 379 K (Figs. 4 (a) and 5 (a)). This is a direct consequence of the $\phi_g(T)$ in Eq. (10) being negative above 379 K. The two elastic constants based on Eq. (11) show hyperbolic tangent trends (Figs. 4 (b) and 5 (b)). The E_{22} and G_{12} terms for the 28 vol.% SMPC at 293 K are 17% and 25% higher than the values of the 17 vol.% composite, and 8% and 12% higher than the 22 vol.% SMPC. The rate of increase of the transverse and shear moduli as a function of the fiber fraction is lower compared to the case of the longitudinal modulus. Since the matrix dominates both transverse and axial moduli, the effect of the reinforcement is smaller.

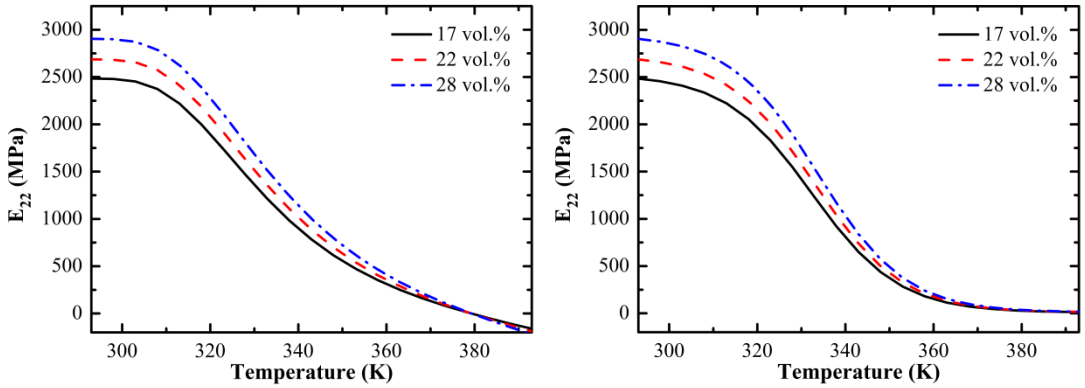

(a) (b)

Fig. 4. Transverse moduli E_{22} of SMPCs at different temperatures, (a) results based on Eq. (10), (b) results based on Eq. (11)

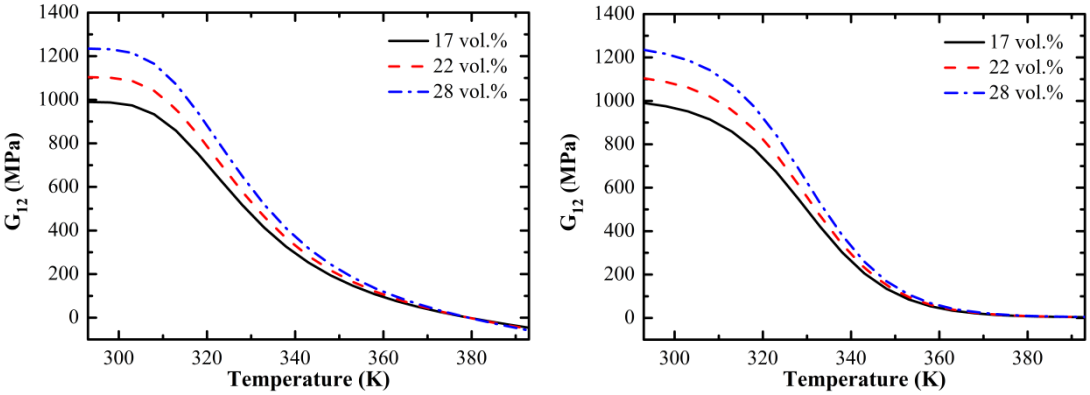

(a) (b)

Fig. 5. Axial shear moduli G_{12} of SMPCs at different temperatures, (a) results based on Eq. (10), (b) results based on Eq. (11)

The axial Poisson's ratio is determined by Eq. (21) and the parameters in Table 1. The Poisson's ratio increases monotonically with the temperature. Because when the matrix is heated, the SMPC becomes softer, resulting in a increase of the Poisson's ratio. The value of the ν_{12} of the SMPC with a lower fiber volume fraction is relatively high, since the matrix contributes more to the mechanical response and the Poisson's ratio of the matrix is higher than that of the fiber.

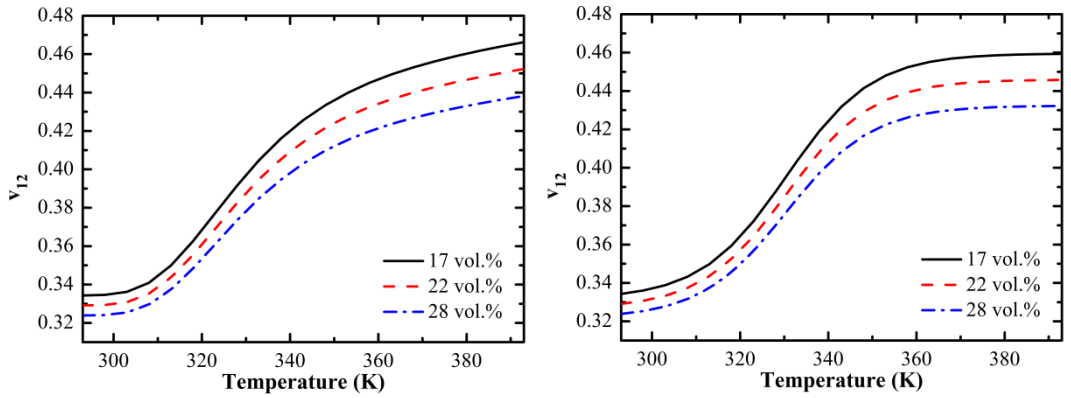

(a) (b)

Fig. 6. Axial Poisson's ratios ν_{12} of SMPCs at different temperatures, (a) results based on Eq. (10), (b) results based on Eq. (11)

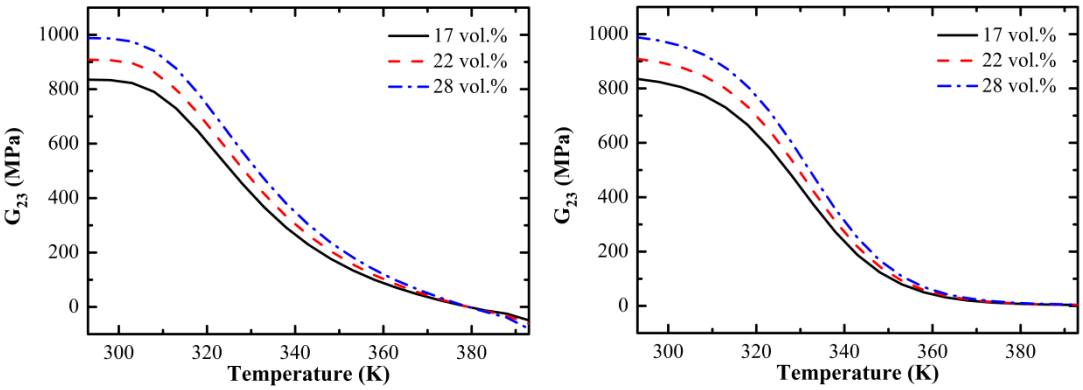

(a) (b)

Fig. 7. Transverse shear moduli G_{23} of SMPCs at different temperatures, (a) results based on Eq. (10), (b) results based on Eq. (11)

The transverse shear modulus G_{23} is obtained by Eq. (22), and follows a temperature dependence similar to the one shown by the in-plane shear modulus, although with lower magnitudes. As the temperature increases through the glass transition region, the distance between the molecules in the matrix increases; the slope of the interatomic potential decreases and therefore results in a reduction of bulk modulus. With the consequent increase of the volume, the molecular mobility becomes larger, leading to a decrease of the shear resistance.

5. Benchmark of the model

To verify the validity of the proposed model we have performed an inverse identification of the elastic constants via numerical and experimental modal analysis of a flat SMPC laminate at temperatures of 293 K, 313 K, 333 K, 353 K, and 373 K. The temperature has been controlled by a resistance heater attached to the laminate. The SMPC laminate is composed of two layers of plain weave carbon fabric (CO6343B, TORAY) with a -45°/45° stacking sequence, and the epoxy-based SMP resin as in reference [Li et al., 2019b]. The laminate has been manufactured via a Vacuum Assisted Resin Infusion (VARI) following the same process as described in reference [Li et al., 2019a]. The fiber volume fraction is ~40.5%. The dimensions of the SMPC laminate are 0.6 mm×50 mm×180 mm. The laminate is partitioned into two portions along the length, the constrained portion has a length of 40 mm, and the outer extension is 140 mm (Fig. 8).

Ply method of the SMPC laminate

No. of layer	Thickness (mm)	Orientation Angle (°)	Material
1	0.14	0	PI
2	0.15	45	SMPC
3	0.15	-45	SMPC
4	0.15	45	SMPC
5	0.15	-45	SMPC

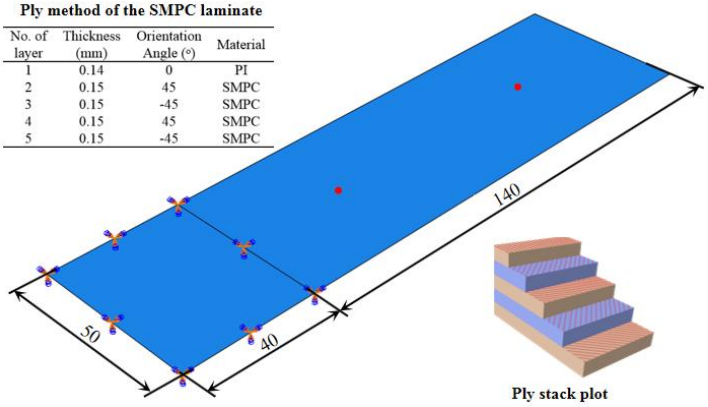

Fig. 8 The finite element model of the flat SMPC laminate

Modal tests are performed using an electro-dynamic shaker with the SMPC laminate fixed on an aluminum base (same as in reference [Li et al., 2019b]). Two thermo couples located at red points in Fig. 8 are used to monitor of the temperature. The dynamic excitation is applied after the temperature stabilized for 5 minutes. A laser doppler velocimetry is used to collect the structural velocity. The setup is shown in Fig. 9. The base vibration acceleration is 0.5 g (1 oct/min) within the 5-500 Hz band. For each temperature, the vibration measurement is performed three times.

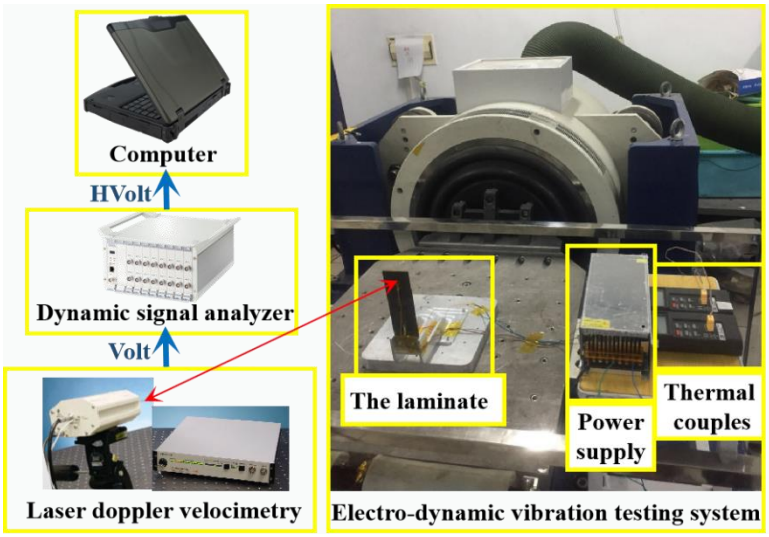

Fig. 9 The modal test setup

The Abaqus Finite Element package has been used to perform the numerical modal analysis. The flat laminate is represented by shell elements. The thickness of the laminate is 0.74 mm with a stacking sequence shown in Fig. 8. The first ply is a polyimide (PI) membrane (Young's modulus of 3.4 GPa, and Poisson's ratio of 0.34) that represents the resistance heater. The elastic constants of a single SMPC layer at varying temperatures are calculated using the proposed analytical model (Table 3). The densities of the PI and the SMPC are 1420 kg/m^3 and 1500 kg/m^3, respectively. The constrained portion is fixed in all directions.

Table. 3 Elastic constants of the unidirectional carbon fiber reinforced epoxy-based SMPC

Temperature (K)	E_{11} (MPa)		E_{22} (MPa)		ν_{12}		G_{12} (MPa)		G_{23} (MPa)	
	$\phi_g(T)$ by Eq. (10)	$\phi_g(T)$ by Eq. (11)	$\phi_g(T)$ by Eq. (10)	$\phi_g(T)$ by Eq. (11)	$\phi_g(T)$ by Eq. (10)	$\phi_g(T)$ by Eq. (11)	$\phi_g(T)$ by Eq. (10)	$\phi_g(T)$ by Eq. (11)	$\phi_g(T)$ by Eq. (10)	$\phi_g(T)$ by Eq. (11)
293	70419	70428	3459	3459	0.31	0.31	1617	1618	1196	1196
313	62106	62183	3173	3176	0.32	0.32	1407	1409	1080	1081
333	32825	33338	1940	1966	0.36	0.36	687	700	623	632
353	14121	9701	837	515	0.39	0.39	246	144	259	158
373	5291	4436	161	89	0.40	0.40	43	23	49	27

The mode shapes of the flat SMPC laminate are similar to the ones of a cantilever beam during the whole temperature interval considered. The first mode is the bending along the axis X (Fig. 10). Table 4 shows the numerical and experimental natural frequencies at different temperatures. With the temperature increases, the natural frequency decreases. In experimental results, the first natural frequency is 13.5 Hz at 293 K. That resonance drops by ~18% to 11.1 Hz at 333 K, and ~64% to 4.8 Hz at 373 K.

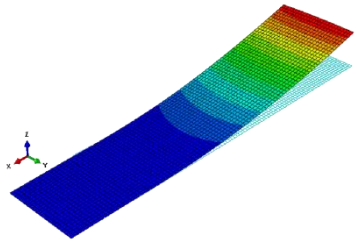

Fig. 10 The first mode shape of the flat SMPC laminate

Table 4. The first order natural frequencies of the laminate at elevated temperatures

Temperature (K)	Natural frequencies (Hz)		
	Numerical		Experimental
	$\phi_g(T)$ by Eq. (10)	$\phi_g(T)$ by Eq. (11)	
293	14.1	14.1	13.5
313	13.4	13.4	12.9
333	10.6	10.7	11.1
353	7.8	6.8	7.5
373	4.9	4.3	4.8

The numerical results with elastic constants based on Eq. (10) are slightly higher than the experimental ones, except at 333 K. The error between numerical and experimental results is less than 4.5% at these temperatures. Small deviations at 293 K and 313 K might due to the fact that

the constraints of actual testings do not perfectly have a clamped condition as in the simulation. The reason behind the higher values predicted by the simulations compared to the experiments is due to the more approximated glassy phase volume fraction estimation at 353 K, 373 K.

Similarly to the simulation results with $\phi_g(T)$ by Eq. (10), the data obtained with $\phi_g(T)$ by Eq. (11) also show higher values compared to the experiments at 293 K and 313 K. The reason is the same as outlined above. The larger than predicted experimental results above 333 K are likely due to the uneven thermal distribution over the laminate. The temperature close to the base is ~5 K lower than the rest of the laminate, which means that the actual stiffness of the laminate is slightly higher compared to the simulation case that relates to a uniform thermal distribution. In all, the numerical results fit well to the experimental ones, and substantially prove the accuracy of the model proposed in this study.

6. Conclusion

A model has been developed to predict the temperature-dependent elastic constants of SMPCs with various fiber volume fractions. The matrix of the SMPC is here considered to possess both rubbery and glassy phases, and the transition between them provides the temperature dependence of the SMPC elastic constants. The glassy phase volume fraction function has been established by two methods, one based on the Eyring equation, the other based on the normal distribution equation. Parameters of the two glassy phase volume fraction functions are derived by fitting the normalized modulus as a function of temperature. The longitudinal moduli at low and high temperatures are calculated by modifying the basic rule of mixture. The final longitudinal modulus as a function of temperature is obtained by combining the moduli at the two ends of the temperature spectrum with the glassy phase volume fraction function. The transverse and axial shear moduli are derived by substituting the matrix's modulus with the glassy phase volume fraction function term into the Halpin-Tsai equation. The transverse shear modulus is obtained by replacing the elastic constants with temperature-dependent terms in the Christensen equation. These moduli decrease monotonically with the temperature increase. For a specific temperature, the higher the fiber volume fraction, the larger the modulus of composite. The axial Poisson's ratio

is obtained by using the rule of mixture. Unlike the modulus dependence over temperature, the Poisson's ratio gradually closes to the value associated with an incompressible configuration due to the high proportion of the matrix. Modal tests of a flat SMPC laminate at various temperatures have been performed for the inverse identification of the composite properties. There are small deviations between the simulation and experimental results, and these errors are acceptable due to differences in boundary and thermal distribution conditions between the simulation and actual experiment. The inverse identification from the modal analysis shows that the proposed prediction model is adequate to describe the temperature-dependent elastic constants of the laminate and can be used to design SMPCs laminate configurations. The model proposed in this work is also suitable for any similar transverse isotropic composites with a glass transition matrix and a reinforcement represented by continuous long fibers. The modulus of the reinforcement must also be independent of the temperature and higher than that of the matrix within the specific temperatures range.

Appendix A. Storage modulus prediction of SMPCs

The dynamic properties of the unidirectional carbon fiber reinforced SMPCs with fiber volume fractions of 17 vol.%, 22 vol.% and 28 vol.% have been measured using the dynamic mechanical analyzer DMA 242 C (NETZSCH Instruments, Germany) in dual cantilever mode for the longitudinal modulus, and tensile mode for the transverse one. The temperature increased from 298 K to 418 K at a heating rate of 3 K/min and a frequency of 1 Hz. For the longitudinal modulus testing the specimens had dimensions of 1.9 mm×4 mm×60 mm with the fiber direction along the main length. The support span was 50 mm, and the amplitude was 20 μm. For the transverse modulus testing, the specimen was 1.9 mm×5 mm×30 mm with fiber direction perpendicular to the main length.

The T_g given by either the maximum slope of the storage modulus or the peak of the loss factor (Tan delta) is higher than the one obtained by using the Zwick three-point bending tests facility mentioned in the main part of the paper. We take the average temperature corresponding to the maximum slope of the storage moduli in both longitudinal and transverse directions as the

final T_g, 350.7 K, which would be used in Eqs. (10, 11, 13) to fit the storage modulus. Although the T_g obtained by the DMA tests varies with the fiber fraction and the testing mode, the difference corresponding to the average T_g is less than 4%. The parameters T_g, k, $\Delta G(T_g)$, C_1, C_2, R and n in Eq. (10) are 340.7 K, 0.001 K^{-1}, 800 J/mol, 16, 500 K, 8.314 J/(mol·K), 0.966, respectively. The parameters ω, $T_{\min}$, T_g in Eq. (11) are 30.4 K, 298 K, and 340.7 K, respectively. The values of E_{T_L} and E_{T_H} in Eq. (13) are the experimental results of the SMPCs at 298 K and 418 K. The numerical results based on the Eyring equation do not fit well above 390 K. While the numerical results are better and fit well in the whole temperature range based on the normal distribution equation.

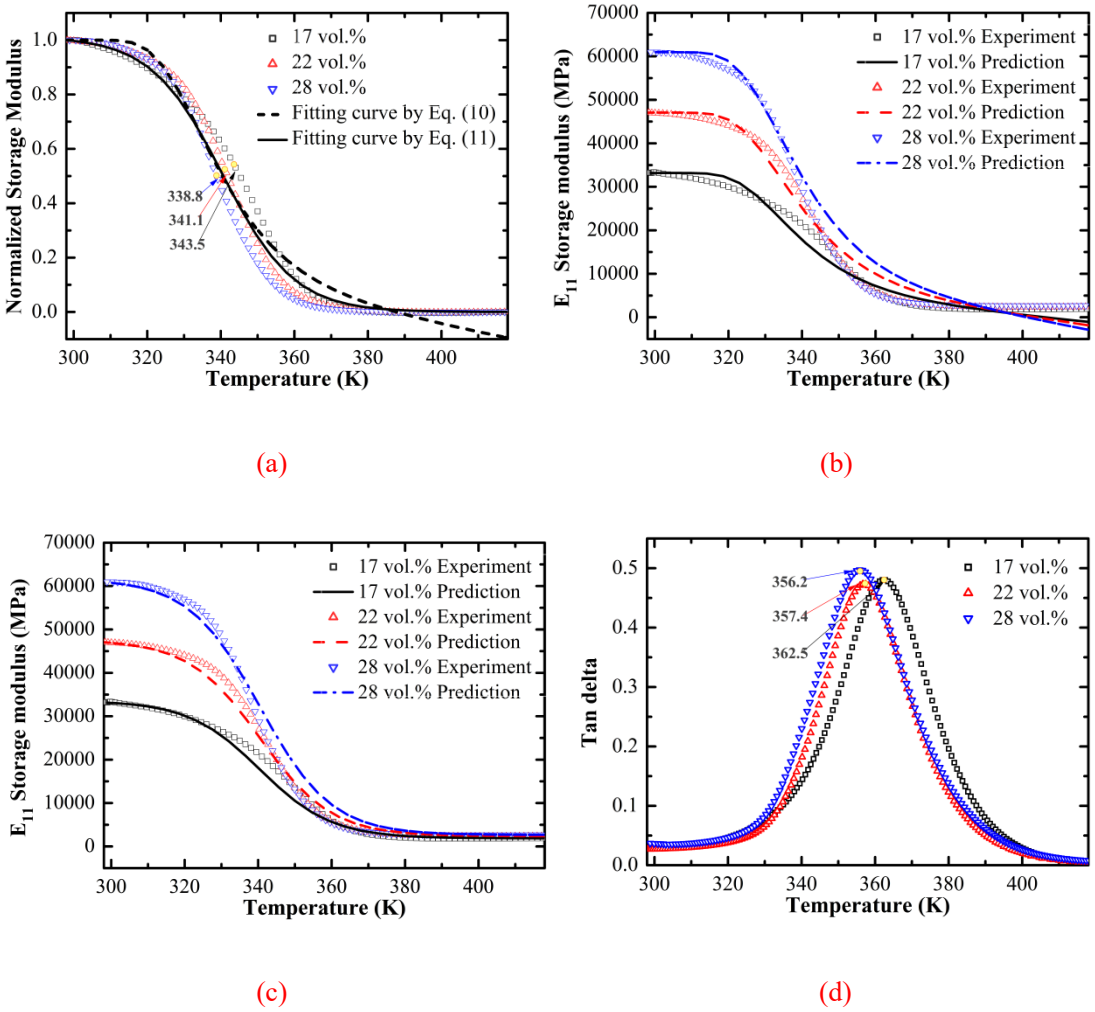

Fig. A.1. DMA results of SMPCs with fiber direction along the specimen's length, (a) normalized

longitudinal storage moduli, (b) longitudinal storage moduli (prediction based on Eq. (10)), (c) longitudinal storage moduli (prediction based on Eq. (11)), (d) tan delta

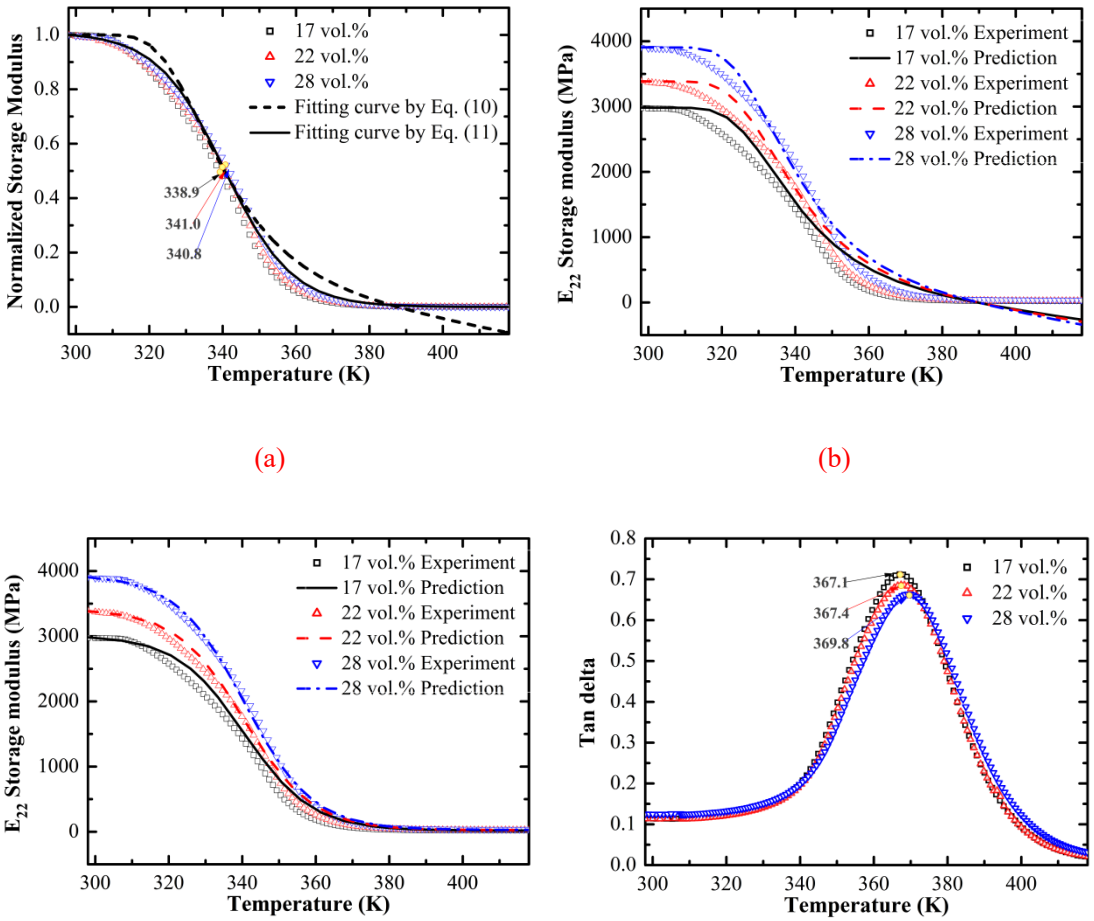

Fig. A.2. The DMA results of SMPCs with fiber direction perpendicular to the specimen's length, (a) normalized transverse storage moduli, (b) transverse storage moduli (prediction based on Eq. (10)), (c) transverse storage moduli (prediction based on Eq. (11)), (d) tan delta

Appendix B. Storage modulus prediction of SMPs

Three SMPs have been selected to calibrate the storage modulus model. The polymers are MMA-co-PEGDMA (with rubbery modulus of 12.8 MPa, and T_g of 76 ºC [Yakacki et al., 2008]), an epoxy-based SMP [Liu et al., 2006] and a styrene-based SMP [Du et al., 2018]. The temperature corresponding to the maximum slope of the storage modulus is identified as the T_g.

Glassy temperature values for these SMPs are 280 K, 317 K and 329 K, respectively. The modulus E_{T_L} is extracted from the experimental data at the lowest temperature of the corresponding curve in Fig. B.1. The values of that modulus are 4250 MPa for the MMA-co-PEGDMA polymer, 1701 MPa for the epoxy-based SMP and 2141 MPa for the styrene-based SMP. The values of E_{T_H} (experimental data at the highest temperature) for these SMPs are 12.8 MPa, 8.5 MPa and 8.3 MPa, respectively. The parameters used in Eqs. (10, 11) are shown in Table B.1. Substituting E_{T_L}, E_{T_H} and $\phi_g(T)$ into Eq. (13) the numerical storage moduli with a R^2 above 95% are shown in Fig. B.1. The numerical moduli show a monotonically decrease with the temperature increase. The numerical moduli identified using the normal distribution equation have a better fit than the ones based on the Eyring equation within the whole temperature range.

Table B.1. The values of the parameters in Eqs. (10, 11)

Parameters	Units	Values		
		MMA-co-PEGDMA polymer	Epoxy-based SMP	Styrene-based SMP
k	[1/K]	0.001	0.001	0.001
$\Delta G(T_g)$	[J/mol]	815.5	1356.7	2057.9
C_1	[-]	16	16	16
C_2	[K]	1062	860	206
n	[-]	1	1	1
ω	[K]	68	44	18
$T_{\min}$	[K]	200	273	297

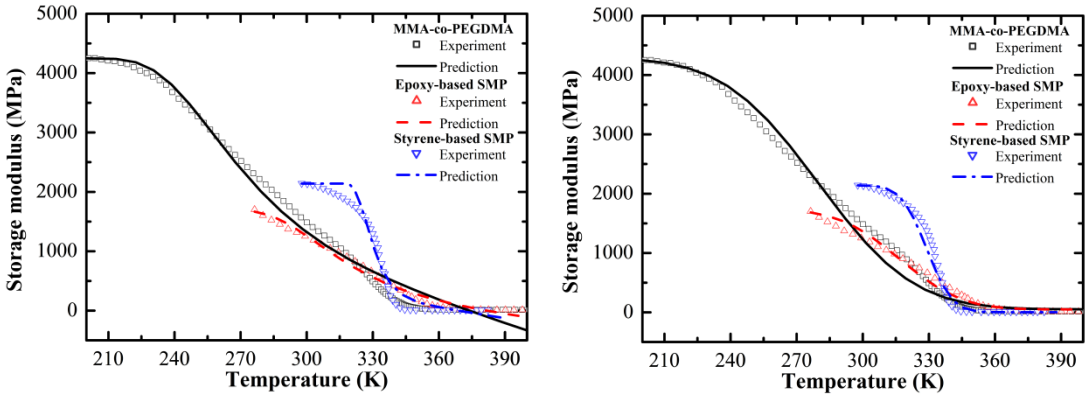

(a) (b)

Fig. B.1. Experimental and numerical results related to the storage moduli of SMPs, (a) prediction based on Eq. (10), (b) prediction based on Eq. (11)

Acknowledgements

This work is supported by the National Natural Science Foundation of China (Grant Nos: 11672086, 11772109 and 11632005).

References

Angell, C.A., 1997. Why C1 = 16-17 in the WLF equation is physical - And the fragility of polymers. Polym. 38, 6261-6266.

Bai, Y., Keller, T., Vallée, T., 2008. Modeling of stiffness of FRP composites under elevated and high temperatures. Compos. Sci. Technol. 68, 3099-3106.

Barnes, J., Cogswell, F., 1989. Thermoplastics for space. SAMPE Q. 20, 22-27.

Barrett, R., Francis, W., Abrahamson, E., Lake, M., Scherbarth, M., 2006. Qualification of elastic memory composite hinges for spaceflight applications, 47th AIAA/ASME/ASCE/AHS/ASC Structures, Structural Dynamics, and Materials Conf. 14th AIAA/ASME/AHS Adaptive Structures Conf. 7th, p. 2039.

Christensen, R.M., 1988. Tensor transformations and failure criteria for the analysis of fiber composite materials. J. Compos. Mater. 22, 874-897.

Dao, T.D., Ha, N.S., Goo, N.S., Yu, W.-R., 2018. Design, fabrication, and bending test of shape memory polymer composite hinges for space deployable structures. J. Intell. Mater. Syst. Struct. 29, 1560-1574.

Dotsenko, V., 1979. Stress relaxation in crystals. Phys. Status Solidi B 93, 11-43.

Du, H., Liu, L., Zhang, F., Leng, J., Liu, Y., 2018. Shape retainability and reusability investigation of bottle-shaped SMP mandrel. Polym. Test. 69, 325-331.

Feng, J., Guo, Z., 2016. Temperature-frequency-dependent mechanical properties model of epoxy resin and its composites. Composites, Part B 85, 161-169.

Gibson, A., Wu, Y.-S., Evans, J., Mouritz, A., 2006. Laminate theory analysis of composites under load in fire. J. Compos. Mater. 40, 639-658.

Gu, P., Asaro, R., 2005. Structural buckling of polymer matrix composites due to reduced stiffness from fire damage. Compos. Struct. 69, 65-75.

Guo, Z.-S., Feng, J., Wang, H., Hu, H., Zhang, J., 2013. A new temperature-dependent modulus model of glass/epoxy composite at elevated temperatures. J. Compos. Mater. 47, 3303-3310.

Haque, A., Mahmood, S., Walker, L., Jeelani, S., 1991. Moisture and temperature induced degradation in tensile properties of Kevlar-graphite/epoxy hybrid composites. J. Reinf. Plast. Compos. 10, 132-145.

Herath, H., Epaarachchi, J., Islam, M., Al-Azzawi, W., Leng, J., Zhang, F., 2018. Structural performance and photothermal recovery of carbon fibre reinforced shape memory polymer. Compos. Sci. Technol. 167, 206-214.

Leng, J., Lan, X., Liu, Y., Du, S., 2011. Shape-memory polymers and their composites: stimulus methods and applications. Prog. Mater. Sci. 56, 1077-1135.

Li, F., Liu, L., Lan, X., Wang, T., Li, X., Chen, F., Bian, W., Liu, Y., Leng, J., 2016. Modal

analyses of deployable truss structures based on shape memory polymer composites. Int. J. Appl. Mech. 8, 1640009.

Li, F., Liu, Y., Leng, J., 2019a. Progress of shape memory polymers and their composites in aerospace applications. Smart Mater. Struct. 28, 103003.

Li, F., Scarpa, F., Lan, X., Liu, L., Liu, Y., Leng, J., 2019b. Bending shape recovery of unidirectional carbon fiber reinforced epoxy-based shape memory polymer composites. Composites, Part A 116, 169-179.

Liu, Y., Gall, K., Dunn, M.L., Greenberg, A.R., Diani, J., 2006. Thermomechanics of shape memory polymers: uniaxial experiments and constitutive modeling. Int. J. Plast. 22, 279-313.

Lu, H., Wang, X., Yao, Y., Fu, Y.Q., 2018. A 'frozen volume'transition model and working mechanism for the shape memory effect in amorphous polymers. Smart Mater. Struct. 27, 065023.

Mahieux, C., Reifsnider, K., 2001. Property modeling across transition temperatures in polymers: a robust stiffness–temperature model. Polymer 42, 3281-3291.

McClung, A.J., Tandon, G.P., Baur, J.W., 2012. Strain rate-and temperature-dependent tensile properties of an epoxy-based, thermosetting, shape memory polymer (Veriflex-E). Mech. Time-Depend. Mater. 16, 205-221.

Mendels, D., Leterrier, Y., Manson, J., 1999. Stress transfer model for single fibre and platelet composites. J. Compos. Mater. 33, 1525-1543.

Miyagawa, H., Sato, C., Mase, T., Drown, E., Drzal, L.T., Ikegami, K., 2005. Transverse elastic modulus of carbon fibers measured by Raman spectroscopy. Mater. Sci. Eng., A 412, 88-92.

Mott, P., Dorgan, J., Roland, C., 2008. The bulk modulus and Poisson's ratio of "incompressible" materials. J. Sound Vib. 312, 572-575.

Odegard, G., Kumosa, M., 2000. Elastic-plastic and failure properties of a unidirectional carbon/PMR-15 composite at room and elevated temperatures. Compos. Sci. Technol. 60, 2979-2988.

Pandini, S., Pegoretti, A., 2008. Time, temperature, and strain effects on viscoelastic Poisson's ratio of epoxy resins. Polym. Eng. Sci. 48, 1434-1441.

Pegoretti, A., Fambri, L., Zappini, G., Bianchetti, M., 2002. Finite element analysis of a glass fibre reinforced composite endodontic post. Biomaterials 23, 2667-2682.

Sauder, C., Lamon, J., Pailler, R., 2004. The tensile behavior of carbon fibers at high temperatures up to 2400 C. Carbon 42, 715-725.

Subramanian, S., 1994. Effect of fiber/matrix interphase on the long term behavior of cross-ply laminates. Ph. D. Thesis. Virginia Polytechnic Inst. and State Univ., Blacksburg, VA (United States).

Volk, B.L., Lagoudas, D.C., Chen, Y.-C., 2010. Analysis of the finite deformation response of shape memory polymers: II. 1D calibration and numerical implementation of a finite deformation, thermoelastic model. Smart Mater. Struct. 19, 075006.

Yakacki, C.M., Shandas, R., Safranski, D., Ortega, A.M., Sassaman, K., Gall, K., 2008. Strong, tailored, biocompatible shape-memory polymer networks. Adv. Funct. Mater. 18, 2428-2435.

Yang, Q., Li, G., 2016. Temperature and rate dependent thermomechanical modeling of shape memory polymers with physics based phase evolution law. Int. J. Plast. 80, 168-186.

Yoon, K.J., Kim, J.-S., 2000. Prediction of thermal expansion properties of carbon/epoxy laminates for temperature variation. J. Compos. Mater. 34, 90-100.